AUTHOR(S):

Shimura, Tomoya; Mori, Nobuhito; Mase, Hajime

Ocean Waves and Teleconnection Patterns in the Northern Hemisphere

TOMOYA SHIMURA

Graduate School of Engineering, Kyoto University, Kyoto, Japan

NOBUHITO MORI AND HAJIME MASE

Disaster Prevention Research Institute, Kyoto University, Kyoto, Japan

ABSTRACT

Understanding long-term, ocean wave climate variability is important to assess climate change impacts on coastal and ocean physics and engineering. Teleconnection patterns can represent wave climate variability in the context of climate change. The objective of this study is to identify how large-scale spatial distributions of wave heights vary on a monthly basis and how they are influenced by various teleconnection patterns using reanalysis datasets. The wave height climate responses to teleconnection patterns in the eastern part of the North Pacific and North Atlantic are more sensible than in the corresponding western parts. The dominant spatial patterns of monthly averaged wave height variability in winter were obtained by empirical orthogonal function analysis. The three dominant patterns in the North Pacific and North Atlantic are similar. It is remarkable that one of the three dominant patterns, a band-shaped pattern, exhibits a strong relation to the teleconnection pattern in each ocean. The band-shaped pattern for the North Pacific was investigated in detail and found to be related to the west Pacific (WP) pattern. Where and how each teleconnection pattern influences wave climate becomes apparent especially during winter.

1. Introduction

Impacts and adaptations of climate change have been studied in various fields. Sea level rise greatly impacts human activity near coastal zones (Bindoff et al. 2007) and amplifies the vulnerability of coastal regions. Ocean surface gravity waves (simply waves hereafter) produce more complex impacts than sea level rise on coastal and ocean structures, beach morphology, and other ecosystems. To assess the impacts of climate change on coastal areas, it is necessary to evaluate how wave climate changes as a result of climate change. The wave climate variability exhibits both long-term trends and oscillations depending on the location. Clarifying characteristics in wave climate variability such as trends and oscillations is important to understand past and future wave climate changes.

The global climate has preferred patterns of variability, which are called teleconnection patterns or large-scale atmospheric circulation patterns. Basically, a teleconnection is made up of a fixed spatial pattern with an associated index time series showing the evolution of its amplitude and phase (Trenberth et al. 2007), which is defined by sea surface temperature (SST), 500-hPa geopotential height ($Z500$), and so on. The teleconnection patterns, such as the El Niño–Southern Oscillation (ENSO), the North Atlantic Oscillation (NAO), and the Arctic Oscillation (AO), are widely considered to be associated with typical climate variability (Trenberth et al. 2002; Hurrell et al. 2003; Thompson and Wallace 1998). It is well known that ENSO has a periodic fluctuation of 2–7 yr (McPhaden et al. 2006) and a profound worldwide effect on the annual climate. Although teleconnection patterns originally, and literally, indicate simultaneous fluctuations of climate values at widely separated points and spatial patterns (Walker and Bliss 1932; Wallace and Gutzler 1981), the discussion about the relationships between the occurrence trends of teleconnection patterns and multidecadal change in the climate state started in the 1990s (e.g., Trenberth 1990; Trenberth and Hurrell 1994; Hurrell 1996; Thompson and Wallace 1998).

For instance, local increases in surface temperature were explained by teleconnection patterns. Hurrell (1996) reported that increasing trends in surface temperatures

---

in Europe and decreasing trends in the northeast Atlantic from the 1970s corresponded to a positive trend of the NAO. Similarly, an increasing trend in surface temperatures in Alaska and a decreasing trend in the North Pacific corresponded to a positive trend of the Pacific–North America pattern (PNA). Trenberth et al. (2002) explained that a 0.06°C increase in globally averaged atmospheric surface temperature from 1950 to 1998 was related to a change in ENSO. The teleconnection pattern indices are useful for climate study as macroscopic indicators of climate variability and multidecadal change in the climate state, rather than the phenomena of teleconnection itself.

As pointed out by several studies (Deser et al. 2012; Hawkins and Sutton 2009; Tebaldi et al. 2011), a major source of uncertainty accompanied with climate projections is the internal natural variability such as decadal or multidecadal oscillations in the system. Therefore, it is important to understand the natural variability, expressed as a teleconnection pattern.

In coastal and ocean engineering, the relationship between wave climate variability and teleconnection patterns has been discussed. The wave climate of the North Atlantic has been more studied than that in the North Pacific. It is well known that the long-term variability of wave heights in the North Atlantic has a strong connection to the NAO (Bauer 2001; Wang and Swail 2001; Woolf et al. 2002; Gulev and Grigorieva 2006; Izaguirre et al. 2010). There are also several studies analyzing the relationship between wave climate in the North Atlantic and teleconnection patterns such as the east Atlantic pattern (EA) (Woolf et al. 2002; Izaguirre et al. 2010), the east Atlantic–western Russia pattern (EAWR), and the Scandinavian pattern (SCA) (Izaguirre et al. 2010).

On the other hand, wave climate in the North Pacific is likely to be associated with the Aleutian low and southern phenomena (e.g., ENSO) (Graham and Diaz 2001; Wang and Swail 2001; Semedo et al. 2011; Izaguirre et al. 2011). The Aleutian low shows a high correlation with the PNA. Thus, the PNA can be a proxy of the wave climate in the North Pacific. The correlation coefficient between the North Pacific index (NPI) and the PNA index is −0.91 in the winter season when the Aleutian low is the deepest (Trenberth and Hurrell 1994).The NPI indicates the magnitude of the Aleutian low. The decadal upward trend of both averaged and extreme wave heights is detected in the midlatitudes of the North Pacific (Graham and Diaz 2001; Wang and Swail 2001; Gulev and Grigorieva 2006; Izaguirre et al. 2011; Semedo et al. 2011), which corresponds to the change due to the climatology of the Aleutian low (Wang and Swail 2001). Menéndez et al. (2008) showed that the

PNA index denotes a rather serious impact on extreme wave climate in the eastern North Pacific based on long-term buoy observations. The significant correlations of wave heights in the northeast Pacific with El Niño (Menéndez et al. 2008; Seymour 2011) and the Pacific decadal oscillation (PDO) (Seymour 2011) were reported.

From the global point of view, Semedo et al. (2011) analyzed the connection between wave and teleconnection pattern indices (denoted by large-scale atmospheric circulation indices in their work) based on the 40-yr European Centre for Medium-Range Weather Forecasts (ECMWF) Re-Analysis ERA-40 dataset. They obtained main patterns of the interannual variability of the swell fields by empirical orthogonal function analysis, and reported a strong relationship between swells and teleconnection patterns. Fan et al. (2012) computed past wave climate using the wave model WAVEWATCH3 coupled with atmosphere model and showed that wave climate exhibits clear relations to the NAO in the North Atlantic and the Southern Oscillation index (SOI) in the Pacific Ocean, respectively. In addition, wave climate and teleconnection patterns in the Southern Hemisphere have been analyzed. Hemer et al. (2010) showed a strong positive correlation between wave climate (wave height) and the southern annular mode (SAM) in the Southern Hemisphere.

Teleconnection patterns are useful indicators of how climate change can impact wave climate variability, and evaluating climate natural variability, which can be expressed as teleconnection patterns, is important for climate projections. This study makes clear the relationship between regional wave climate variability and teleconnection patterns so that wave climate will be addressed in context of natural variability and climate change through teleconnection patterns. Most of the previous studies mentioned so far have focused on how wave climate variability observed at certain locations can be explained by teleconnection patterns, or on how spatial patterns of wave climate variability derived from satellites, hindcasts, or reanalysis data correlate with teleconnection patterns. In other words, previous studies have focused on how given wave climate variability can be explained by limited teleconnection patterns. Therefore, spatial scopes of influence by teleconnection patterns and how the influences overlap spatially are not well known, especially in the North Pacific. In this study, we start with a given and general teleconnection pattern to see how it affects wave climate variability in the Northern Hemisphere. The spatial distributions of wave climate variability influenced by teleconnection patterns are addressed. We use not only teleconnection patterns that are known to be related with wave climate but also teleconnection patterns that have been rarely used in

wave climate study because the target area is the entire Northern Hemisphere; there is no reason to use limited teleconnection patterns. This analysis will also examine whether wave climate variability can be estimated from teleconnection patterns using a linear multiple regression model, without the use of a dynamic model. In addition, the winter wave climate in the North Pacific and the North Atlantic is statistically analyzed in detail by using an empirical orthogonal function (EOF) analysis. Deeper analyses are conducted with the winter wave climate in the North Pacific since there is less evidence based on previous studies for the North Atlantic. For this paper, only the Northern Hemisphere is analyzed, and the analysis for the Southern Hemisphere will be conducted in a subsequent paper.

This paper is organized as follows. In section 2, datasets and procedures for making teleconnection pattern indices are described. Results are shown in section 3, which consists of five subsections: (a) seasonal differences, (b) spatial characteristics of teleconnection pattern influences on winter wave climate variability, (c) wave height predictability by index, (d) the relationship between main spatial patterns of wave climate variability and teleconnection patterns, and (e) detailed analysis of winter wave climate variability in the North Pacific. This paper concludes with section 4.

2. Analyzed data and teleconnection pattern indices

a. Datasets

Two different analytical datasets were used in this study. One is the National Centers for Environmental Prediction (NCEP)–National Center for Atmospheric Research (NCAR) reanalysis dataset (Kalnay et al. 1996). The spatial resolution is 2.5° latitude and longitude. Monthly averaged data from 1950–2000 were used: 500-hPa geopotential height, sea level pressure (SLP), and SST. In section 3e only, $Z500$ data to 2009 were used. The NCEP–NCAR reanalysis dataset was used to develop reference teleconnection patterns following the method of the Climate Prediction Center (CPC) of the National Oceanic and Atmospheric Administration (NOAA), which is described in detail in section 2b.

The other dataset is the ERA-40 reanalysis data (Uppala et al. 2005) supplied by the European Center for Medium-Range Weather Forecasts. Spatial resolution is 2.5° latitude and longitude. Monthly averaged data for Z500, SLP, SST, and significant wave height (SWH) covering 1960–90 were used. In section 3e only, monthly averaged data for $Z500$ and 6-hourly SLP up to 2001 were used. The reason the period 1960–90 was

adopted in this analysis is that although ERA-40 reanalysis is provided to August 2002, the SWH data of ERA-40 are inhomogeneous before and after the assimilation of altimeter wave height data in the 1990s (Sterl and Caires 2005). Sterl and Caires (2005) showed that although ERA-40 underestimates wave heights, particularly the high wave heights, the monthly mean wave fields compare well with observations. The Z500, SLP, and SST data were used to make teleconnection pattern indices in ERA-40 based on reference teleconnection patterns derived from the NCEP–NCAR reanalysis, described in detail in section 2b. The relationships between the indices and the monthly averaged SWH were analyzed.

We used a coarser version of ERA-40 (2.5° resolution) but the spatial resolution of the ERA-40 original version is 1.5°. Furthermore, Sterl and Caires (2005) have produced the corrected ERA-40 wave data, showing the clear improvement of the quality as well as the removal of the inhomogeneities due to changes in altimeter wave height assimilation. Therefore, the use of the coarser version of ERA-40 during 1960–90 is not considered optimal. However, we conducted the same analysis using the ERA-40 original version during 1960–90 and corrected ERA-40 data (Sterl and Caires 2005) during 1960–90 and 1958–2001, and we got almost the same results as with the coarser version of ERA-40 during 1960–90.

b. Teleconnection pattern indices

We selected nine teleconnection patterns defined by the $Z500$ data for analysis: 1) the North Atlantic Oscillation, 2) the East Atlantic pattern, 3) the east Atlantic–western Russia pattern, 4) the Scandinavian pattern, 5) the polar–Eurasian pattern (POL), 6) the west Pacific pattern (WP), 7) the east Pacific/North Pacific pattern (EPNP), 8) the Pacific–North American pattern, and 9) the tropical–Northern Hemisphere pattern (TNH). These patterns are well reviewed in Panagiotopoulos et al. (2002) and have been monitored by the CPC (http://www.cpc.ncep.noaa.gov/data/teledoc/telecontents.shtml).

As described in the introduction, the NAO and PNA are considered to be well associated with wave climate variability in previous studies (Wang and Swail 2001; Woolf et al. 2002; Gulev and Grigorieva 2006; Izaguirre et al. 2010). There are no universally accepted criteria and procedures to define the NAO, PNA, and other teleconnection patterns (Panagiotopoulos et al. 2002). The CPC monitors the behavior of teleconnection patterns and defines these patterns based on the method of Barnston and Livezey (1987), applying one of the EOF analyses, rotated empirical orthogonal function (REOF) analysis, to the $Z500$ data. As a result of REOF analysis, nine components of Z500 variability are defined simultaneously

TABLE 1. Correlation coefficients between indices derived from ERA-40 and NCEP–NCAR reanalysis. The period is 1960 to 1990. TNH is only for winter.

	NAO	EA	WP	EPNP	PNA	EAWR	SCA	TNH	POL	Niño-3.4	AO
Winter (DJF)	0.995	0.982	0.992	0.993	0.996	0.993	0.995	0.998	0.986	0.990	0.996
Spring (MAM)	0.995	0.962	0.995	0.996	0.996	0.971	0.974	—	0.984	0.980	0.988
Summer (JJA)	0.990	0.935	0.990	0.992	0.908	0.957	0.965	—	0.993	0.986	0.954
Autumn (SON)	0.994	0.983	0.989	0.996	0.996	0.932	0.995	—	0.994	0.991	0.958

as teleconnection patterns mentioned above, including the NAO and the PNA.

The relationships between the spatial patterns of the wave climate and teleconnection patterns are not well understood at present. Therefore it is not reasonable to use only the PNA, NAO, or limited patterns as teleconnection patterns for a wave climate study despite the fact that the other patterns mentioned above can be defined as components of $Z500$ variability, in the same way that NAO and PNA can be defined by REOF analysis. In this study, all of the teleconnection patterns that are introduced as prominent teleconnection patterns over the Northern Hemisphere on the CPC web site were considered. However, the Pacific transient pattern (PT) was eliminated because the PT covers August to September, and the analysis in this paper mainly focuses on the winter season.

The numerical procedures to define teleconnection patterns are described as follows. The reference teleconnection patterns were developed from the NCEP–NCAR reanalysis following the method of CPC, before teleconnection pattern indices were made from the ERA-40 reanalysis. First, the NCEP–NCAR reanalysis monthly averaged $Z500$ values for the Northern Hemisphere (northward from 20°N) for years 1950 to 2000 were normalized using the corresponding monthly average values and their standard deviations. Second, the spatial differences in latitudes (ϕ) were considered. On the equator, where ϕ equals zero, the number of grid points per distance is $n/(2\pi R)$, where R is the earth's radius and n is the number of grid points in longitude. On a given latitude ϕ, the number of points is $n/(2\pi R \cos\phi)$. To equalize the contribution of each grid point with the total variance in the whole domain, data at each grid point are multiplied by $\sqrt{\cos\phi}$. This procedure is described as the latitudinal correction hereafter. Finally, REOF analysis (von Storch and Zwiers 2002, 305–309) was applied to the covariance matrix ($\mathbf{V}$) of the normalized and latitudinal corrected $Z500$ data. The eigenvalue equation for $\mathbf{V}$ can be expressed as $\mathbf{V}\mathbf{z}_i = \lambda_i \mathbf{z}_i$ with the ith largest eigenvalue λ_i and the associated ith eigenvector $\mathbf{z}_i$. Here, $|\mathbf{z}_i| = 1$. Then, the REOF modes matrix ($\mathbf{Q}$) can be expressed as $\mathbf{Q} = (\mathbf{q}_1 \ldots \mathbf{q}_k) = \mathbf{ZR}$, where $\mathbf{q}_i$ is the ith REOF mode, $\mathbf{Z}$ consists of k eigenvectors ($\mathbf{z}_1 \ldots \mathbf{z}_k$) and $\mathbf{R}$ is an orthonormal rotation matrix defined by the varimax method (Kaiser 1958). In this case, $k = 10$. These nine REOF modes (out of 10) were defined as teleconnection patterns mentioned above by comparing the spatial distributions of the REOF modes with teleconnection patterns shown by the CPC. These nine REOF modes were stored as reference teleconnection patterns. The time coefficient a_t of REOF mode ($\mathbf{q}_i$) at a given time (t) was calculated by projecting the normalized and latitude-corrected $Z500$ data at t ($\mathbf{w}_t$) onto $\mathbf{q}_i$, such that $a_t = \mathbf{w}_t \mathbf{q}_i$. Coefficient a_t for the ERA-40 reanalysis was calculated by projecting the ERA-40 $Z500$ data onto the reference teleconnection patterns. The coefficient a_t was defined as a teleconnection pattern index. The time series of indices derived from ERA-40 is, in hindsight, almost the same as that from the NCEP–NCAR reanalysis (Table 1).

The procedures to calculate the teleconnection pattern indices described above can invite the following two questions. Why use two reanalyses? Why not apply the REOF analysis directly to the ERA-40 data? The answers are addressed below.

1) The NCEP–NCAR reanalysis covers a longer period than the ERA-40.
2) The definition of teleconnection patterns is based on that of the CPC using NCEP–NCAR reanalysis.
3) It is useful to store reference teleconnection patterns when you want to obtain teleconnection pattern indices from a global climate model (GCM); you can get the index easily and consistently by projecting the GCM $Z500$ data onto the reference teleconnection pattern instead of applying REOF analysis. Consistently means that indices derived from GCMs are associated with an identical spatial pattern, a reference pattern. If REOF analysis is applied to certain GCM data, it cannot be guaranteed to derive an identical pattern in reanalysis. We will examine the relationship between wave climate variability and teleconnection patterns derived from a GCM in future research.

In addition to nine teleconnection patterns, two other teleconnection patterns that are widely associated with climate variability were used. One is the Arctic Oscillation, which is the first mode of the EOF for SLP in the
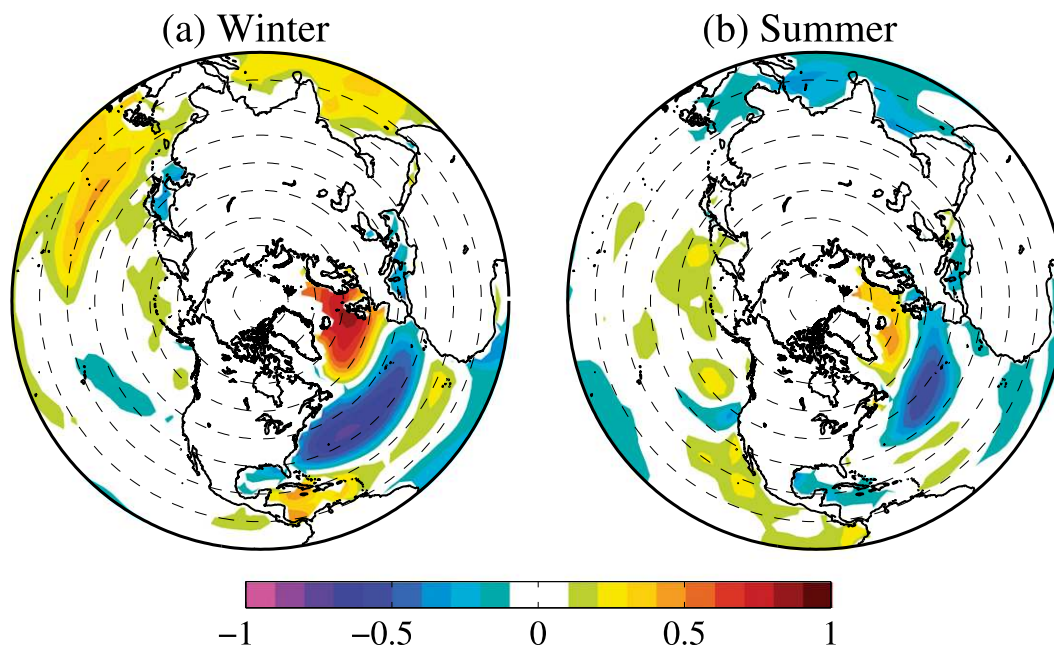
FIG. 1. Spatial distributions of the correlation coefficients between the NAO index and monthly averaged SWH.

Northern Hemisphere north of 20°N (Thompson and Wallace 1998). Indices of the AO in the ERA-40 data were calculated by projecting the ERA-40 SLP data onto the reference pattern derived from the NCEP–NCAR reanalysis. The second is El Niño, which is defined as the anomalies of SST in the Niño 3.4 region from 5°N to 5°S and from 170° to 120°W. This index is denoted Niño-3.4.

3. Results and discussions

a. Seasonal differences

It is well known that wave climate has seasonal variations depending on the hemisphere. Both the wave climate and teleconnection patterns are sensitive to the season, which is discussed first. Here, winter is defined as the months December–February (DJF). Following the same manner spring, summer and autumn are defined as the months March–May (MAM), June–August (JJA), and September–November (SON), respectively. As an example, the spatial distributions of the correlation coefficients between the NAO index and the monthly averaged SWH in winter and summer are shown in Fig. 1. Although these two distributions from different seasons in the North Atlantic are similar to each other, the absolute values of the correlation coefficients in winter are generally greater than in summer (Fig. 1). We examined similar analyses for other teleconnection patterns. The absolute values of the correlation coefficients in the

Northern Hemisphere during the winter are the highest, and those during the summer become the lowest, with some exceptions in a few regions and a few indices.

The reason why teleconnection patterns are more related to wave climate variability in the winter is addressed below. Atmospheric pressure in the Northern Hemisphere varies more during the winter compared with other seasons, generally. The total variances of monthly averaged $Z500$ in the Northern Hemisphere (poleward from 20°N) from the ERA-40 data from 1960–90 for the months January through December are 1.00, 1.00, 0.79, 0.52. 0.37, 0.31, 0.25, 0.28, 0.37, 0.48, 0.65, and 0.85, respectively. Here, latitudinal correction is applied, and the values are normalized with the January value. For SLP, the values are 1.00, 0.75, 0.42, 0.24, 0.19, 0.16, 0.21, 0.27, 0.39, 0.55, and 0.73. Furthermore, for winter, teleconnection patterns can explain the variance to a greater extent than for the other seasons. The percent variances for all seasons are shown in Table 2. The total percent variances among all of the teleconnection patterns derived from $Z500$, except for TNH, are 57.6%, 46.6%, 43.1%, and 47.0% from winter to autumn, respectively. As the result of correlation analysis between the monthly averaged SLP and $Z500$ (not shown), it was found that the way SLP varies in winter corresponds more to how $Z500$ varies over the ocean on a monthly basis than other seasons. Wang and Swail (2006) showed that SWH variations are closely associated with contemporaneous SLP variations. As described above, in winter, when atmospheric variations such as $Z500$ and

TABLE 2. Percent variances of teleconnection patterns (%). The values for AO are based on variance in SLP and others are based on $Z500$. Those for Niño-3.4 cannot be derived. The TNH variance is only for winter.

	NAO	EA	WP	EPNP	PNA	EAWR	SCA	TNH	POL	Niño-3.4	AO
Winter (DJF)	9.1	6.1	9.0	6.4	7.7	6.8	5.3	6.4	7.2	—	17.9
Spring (MAM)	6.9	4.3	6.3	4.9	5.0	5.5	5.6	—	8.1	—	15.1
Summer (JJA)	6.6	5.4	4.6	5.1	8.1	4.1	4.7	—	4.5	—	12.3
Autumn (SON)	6.3	4.8	5.2	5.5	6.4	4.9	6.8	—	7.1	—	12.0

SLP are the greatest, teleconnection patterns dominate the atmospheric variations and $Z500$, SLP, and SWH are associated well. Therefore, it is not surprising that the correlation coefficients between teleconnection pattern indices and SWH in the Northern Hemisphere during winter are the largest of the year. From this point of view, El Niño is also similar despite being defined by SST, because the SST variation is the highest during the winter and is accompanied by a fluctuation in atmospheric pressure, leading to a fluctuation in wave heights.

Although Semedo et al. (2011) reported a strong connection between main patterns of the interannual variability of the swell fields and teleconnection patterns, the coexistence of swells and wind waves complicates the relationship between wave height and teleconnection pattern because wind waves and swells have different sources of wave generation geographically. In addition, it can be easily expected that wind waves are related to teleconnection patterns rather than swell because teleconnection patterns affect winds in advance of ocean waves. Swells dominate ocean waves more in the summer as compared to the stormy winter season. This is one of the reasons why teleconnection patterns are less related to wave climate variability in summer.

Thus we will focus on the stormy winter season when wave climate variability has a stronger relation to teleconnection patterns as shown above.

b. Spatial characteristics of teleconnection pattern influences on winter wave climate variability

First, significance is defined. The total number of months of data for the analysis is 93 (31 yr × 3 months) for each grid point. If the data are independent and the correlation coefficient is larger than 0.2, a null hypothesis indicating no correlation is rejected by the 5% significance level. However, the series of monthly data in a certain year cannot be assumed to be independent. Therefore, the 3-month dataset for winter is regarded as one unit and the number of independent datasets is assumed to be 31, corresponding to the number of years. Following standard statistical analysis, when the correlation coefficient is larger than 0.36, the correlation is considered to be significant by the 5% significance level.

The distributions of correlation coefficients between all the teleconnection patterns derived from $Z500$ and monthly averaged SWH were computed and shown in Fig. 2. In addition, the regions that indicate statistically significant correlation with teleconnection pattern indices are all shown in Fig. 3. In some areas, the influences of several teleconnection patterns overlap, illustrating how the complex relationship between wave climate and teleconnection patterns depends on the geographical location. In addition, Fig. 4 shows maps of correlation coefficients for the AO and Niño-3.4 that are widely associated with climate variability.

The spatial distributions of correlation coefficients with respect to each teleconnection pattern have physical meanings such as a winter storm, tropical cyclone, etc. Therefore, the large-scale relationship between wave climate and teleconnection patterns can help illustrate the local-scale relationship both statistically and physically. Both the North Pacific and the North Atlantic, regions that have significant correlation, are larger in the eastern regions than in the western parts (Fig. 3). This is caused by the smaller spatial fluctuations in the atmosphere that are dominant over the land–sea interface where westerly winds move eastward from the continent. The western parts of the SLP or U10 are strongly influenced by land, which disturbs the smooth relationship between the local wind and wave fields (e.g., Tokinaga and Xie 2011). Wang and Swail (2006) and Graham et al. (2013) developed statistical wave models to predict seasonal wave height statistics (average and extreme) using SLP as predictors. They show the model performances in their respective papers: see Fig. 2a in Wang and Swail (2006) and Fig. 10a in Graham et al. (2013). Their models' performances at predicting wave heights are relatively low in western regions rather than eastern regions, which indicates that it is not easy to express wave height variability in the western regions by atmospheric values such as SLP. This supports the spatial distribution in Fig. 3, which shows larger areas of significant correlation in the eastern areas.

The spatial distributions of the SWH climate variability corresponding to teleconnection patterns derived from reanalysis can be compared with the observed data (spatially limited) as follows. In the North Atlantic, both
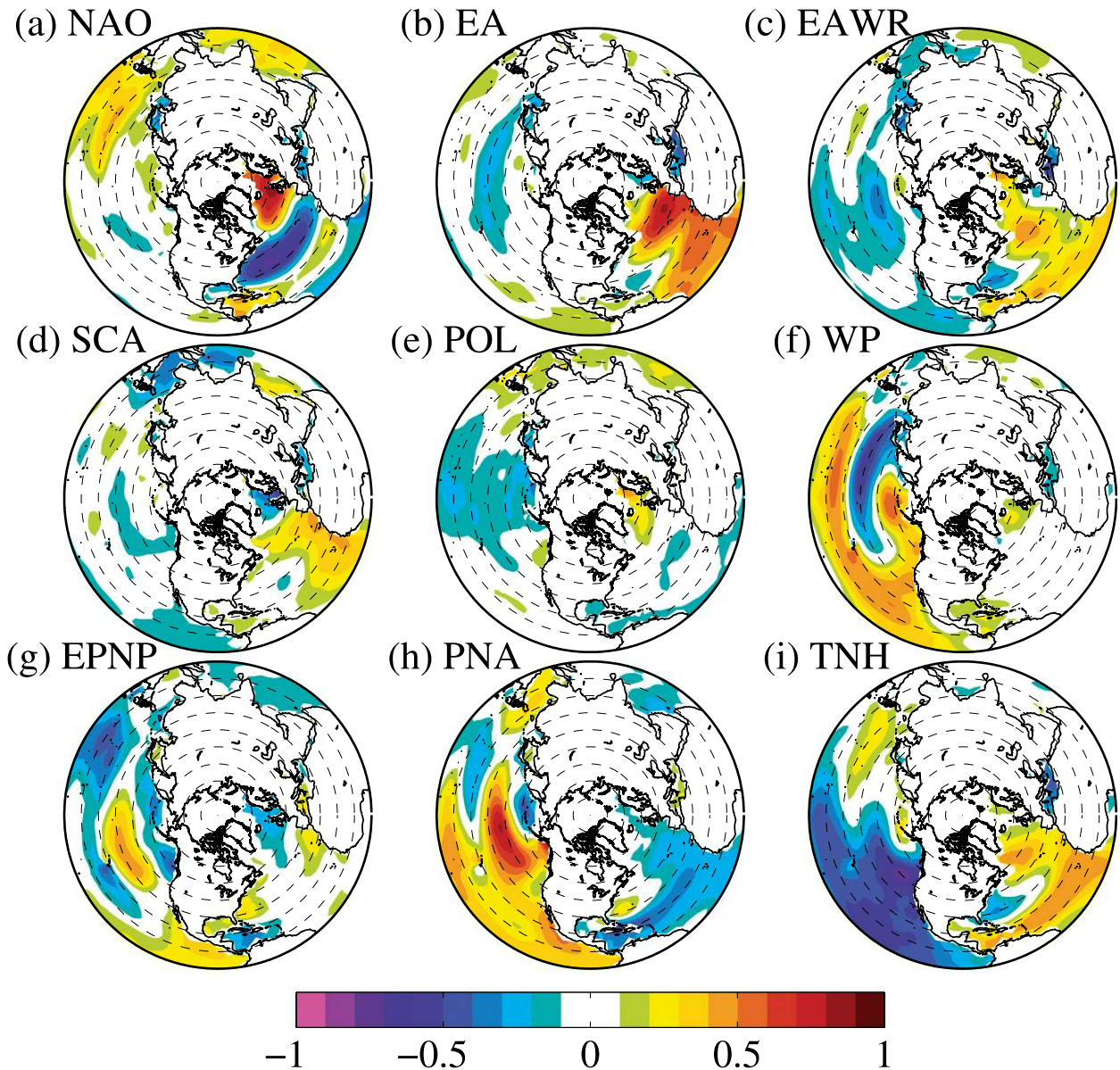
FIG. 2. Spatial distributions of correlation coefficients from *Z*500-based teleconnection pattern indices and monthly averaged SWH in winter.

the NAO and EA indices impact wave climate variability strongly. The spatial distribution of correlation coefficients between winter monthly averaged SWH and the NAO index is characterized by negative values over the region from 30° to 40°N and positive values northward of 50°N (Fig. 2a). This result is consistent with that of satellite observations (Woolf et al. 2002; Izaguirre et al. 2010).

The spatial distribution of correlation coefficients related to the NAO index is similar to that of the AO index (Figs. 2a and 4a) because the NAO and AO indices are

correlated with each other (the correlation coefficients are 0.80, 0.58, 0.60, and 0.73 in winter, spring, summer, and autumn, respectively).

The EA index correlates positively with respect to the SWH in the eastern North Atlantic and negatively in the Mediterranean (Fig. 2b). Although ERA-40 wave data are too coarse to allow conclusions with regard to regional enclosed seas such as the Mediterranean Sea, ERA-40 wind speeds over the Mediterranean Sea correlate negatively with the EA index (not shown). Regarding extreme wave climate, the extreme distribution function model
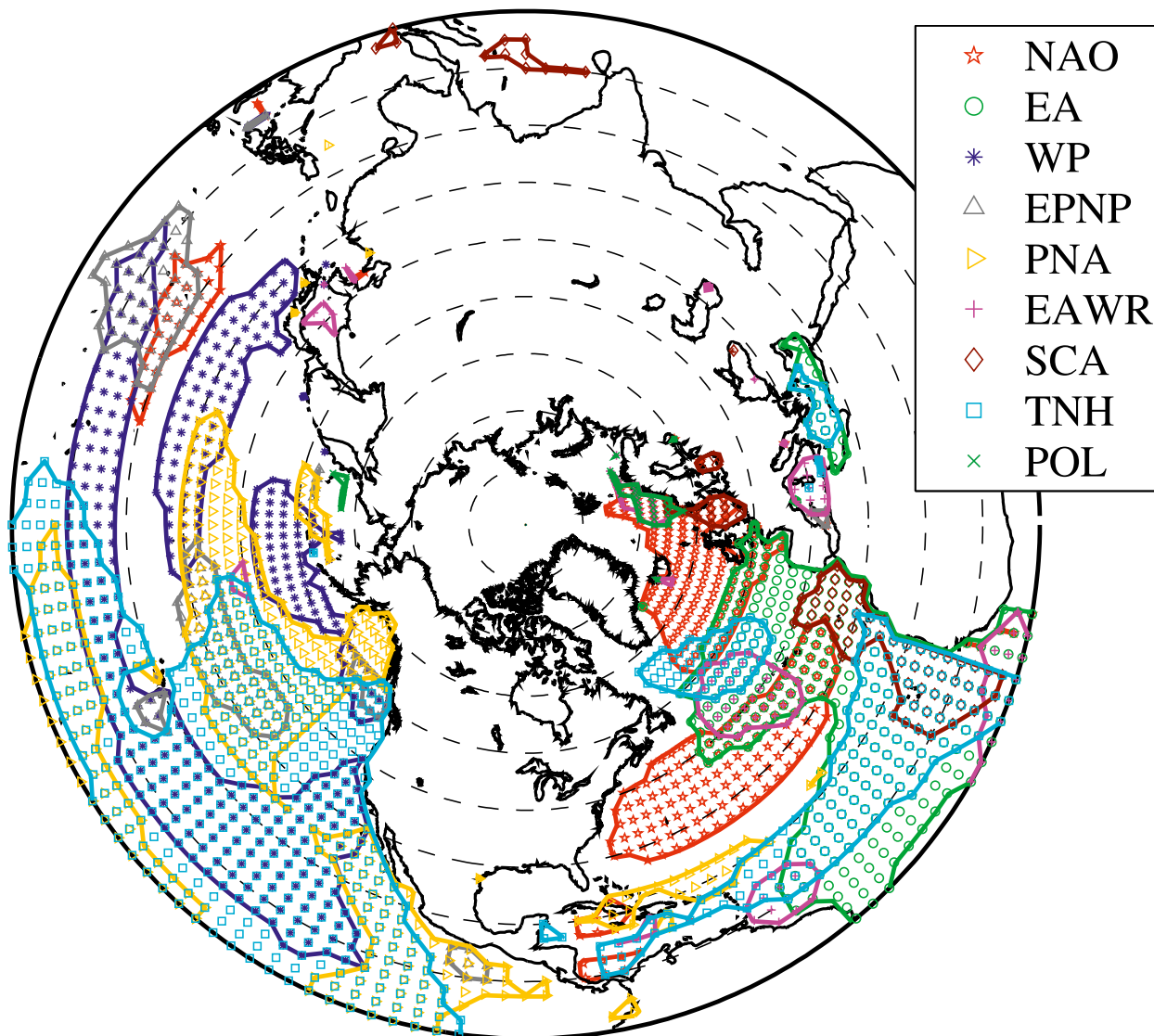
FIG. 3. Areas of significant correlation at the 5% significance level between $Z500$-based teleconnection pattern indices and monthly averaged SWH in winter.

of wave height around the North Atlantic was discussed by Izaguirre et al. (2010). The location parameter expressed as a function of the EA index has a spatial pattern similar to the one for this study (Izaguirre et al. 2010). Also, the results for the EAWR and SCA in Izaguirre et al. (2010) are consistent with this study (Figs. 2c,d).

On the other hand, the PNA, TNH, and WP have greater impact on wave climate variability in the North Pacific. The PNA index correlates positively with the SWH in the eastern half and is especially strong in the center of the North Pacific area (Fig. 2h). Menéndez et al. (2008) show that the PNA influences the extreme wave heights in the eastern North Pacific. The TNH also produces strong influences over the eastern North

Pacific (Fig. 2i). The TNH has greater impact on more eastern regions when compared with the PNA. Therefore, the TNH is the major index for the winter wave climate along the west coast of the United States, rather than the PNA.

Regarding the western North Pacific, Mase et al. (2009) analyzed field observed SWH data along the coast of the Sea of Japan and showed that the correlation coefficients between the AO index and the annual maxima of SWH are about -0.1 to -0.4. Our analysis shows that the correlation coefficients between winter monthly averaged SWH and the AO (or NAO) index are about -0.4 to -0.3 in the Sea of Japan. The spatial pattern of correlation coefficients between the WP index

京都大学
KYOTO UNIVERSITY

8662　　　　　　　　　　　　J O U R N A L   O F   C L I M A T E　　　　　　　　　　　VOLUME 26

京都大学学術情報リポジトリ
KURENAI 紅
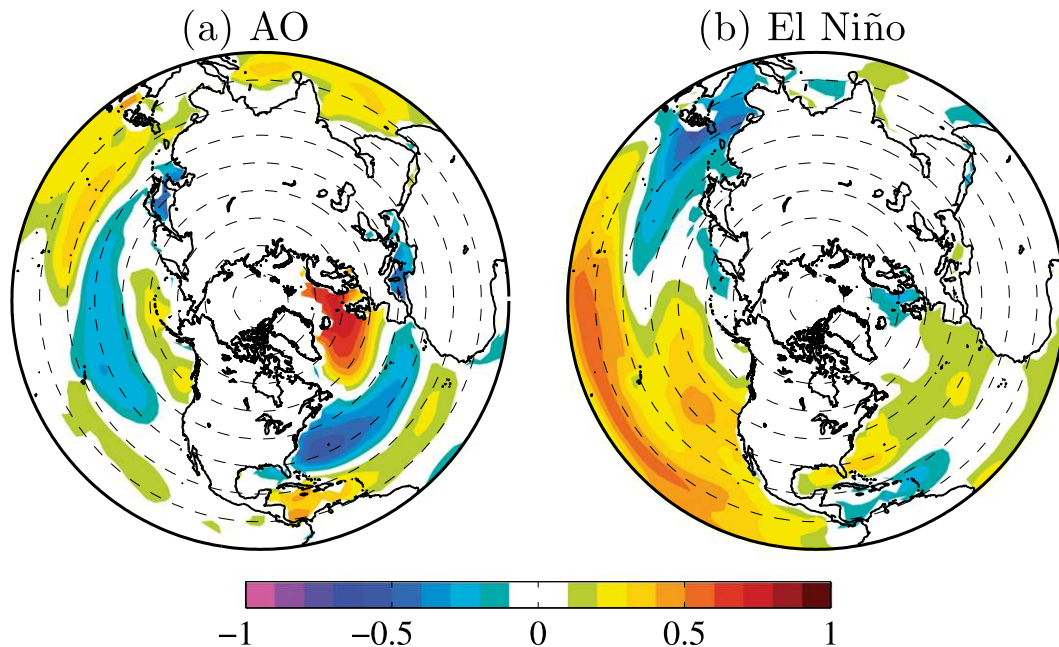Kyoto University Research Information Repository

FIG. 4. As in Fig. 2, but for AO and El Niño.

and the SWH is band-shaped (Fig. 2f), indicating positive, negative, and positive values in low, middle, and high latitudes in the western North Pacific, respectively. The relationship of the TNH and WP with wave climate has not been discussed in previous studies.

For Niño-3.4, the distribution of correlation coefficients with the SWH can be characterized by negative values in the western North Pacific and positive values in the eastern regions. The correlation coefficients are about ± 0.5 in the lower latitudes, and higher values are not observed northward of 20°N (Fig. 4b). Menéndez et al. (2008) indicate that the relationship between extreme wave height in the eastern North Pacific and El Niño is weak but that a positive correlation is significant.

The spatial characteristics of how teleconnection patterns impact wave climate are consistent with the observations of previous studies referred to in this subsection.

c. Prediction of wave climate pattern based on teleconnection pattern index

The predictability of winter averaged SWH from a combination of teleconnection pattern indices is discussed in this section. Teleconnection indices derived from Z500 data, for the nine indices, were used as predictors because the nine indices are nearly uncorrelated from each other. The prediction was examined by linear multivariable regression analysis. A linear regression model was developed for each grid point. The linear regression model is expressed as $y = b + \sum_{i=1}^{k} a_i x_i$, where a_i and b are constants determined by the least squares

method, y is the SWH given as output, and x_i is the index as predictor. The number (k) and the combination of indices as predictors for each grid point were determined based on the Akaike information criterion (Akaike 1973). Predictable skills were determined by cross-validation.

A total of 93 months (3 months $\times$ 31 yr) were split into 78 months (26 yr) as the training period and 15 months (5 yr) as the prediction period. The start year for the prediction period was changed in 5-yr intervals from 1961 to 1986 (1961, 1966, ... , 1986) and the period of training was designated as the rest of the period from 1960 to 1990. Training and prediction were conducted for each corresponding prediction period. Therefore, 90 prediction values (3 months $\times$ 5 yr $\times$ 6 predictions) for each grid point were produced.

Figure 5a shows the correlation coefficients between the ERA-40 winter monthly averaged SWH and the prediction. The correlation coefficients are higher in the eastern part of the ocean basin, especially in the regions where the NAO, EA, and PNA correlate strongly with the SWH (cf. Figs. 5a and 2). In the areas around 20° and 40°N in the western part of the North Pacific and 20°N in the western part of the North Atlantic, the prediction skills are low, and some of these areas show negative correlation values. As an example of the prediction, Figs. 5b and 5c show ERA-40 winter averaged SWH during the period 1986–90 and the prediction. The values in Figs. 5b and 5c are standardized by the mean and standard deviations of the training period 1960–85.
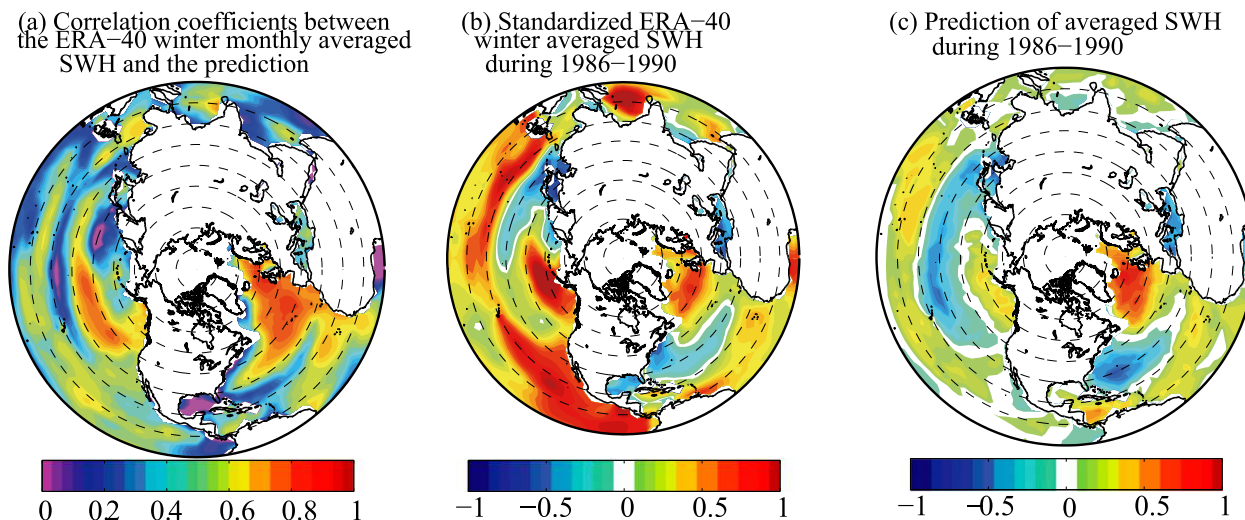
FIG. 5. Prediction performances for monthly averaged SWH in winter based on teleconnection pattern indices.

Tendencies of the prediction (Fig. 5c) show some agreement with those of ERA-40 SWH (Fig. 5b) qualitatively, such as increases in SWH along 15°N, decreases along 30°N, and increases along 55°N in the North Pacific, and NAO-like changes in the North Atlantic. However, quantitatively the predicted values do not agree with ERA-40 SWH values well, especially in the North Pacific. It is possible to improve the accuracy of the prediction by using advanced analysis such as a nonlinear regression instead of a linear one. However, we would like to emphasize that the monthly averaged SWH can be estimated roughly from a combination of climate indices depending on the location. This can provide some applications for wave climate research to predict wave heights roughly with less computational cost than using a dynamic projection base on a physical wave model.

d. The main spatial patterns of wave climate variability and teleconnection patterns

The SWH at each grid point contains various components of fluctuation. Several main components of spatial fluctuation were derived and associated with teleconnection patterns as follows. The EOF analysis was applied to winter monthly averaged SWH in both the North Pacific and the North Atlantic, and the dominant spatial patterns of fluctuation were derived. We defined the North Pacific as the area 0°–60°N, 100°W–100°E and the North Atlantic as the area 0°–70°N, 90°E–20°W. EOF analysis was applied to 93 serial datasets (31 yr × 3 months) during the period 1960–90 for the North Pacific and the North Atlantic separately. Procedures of standardization and latitudinal correction were conducted in the same way as in section 2b before EOF analysis.

Figure 6 shows spatial patterns derived by EOF analysis. The spatial patterns shown are the patterns of the correlation coefficients between the temporal coefficient of the EOF and the monthly averaged SWH. The reason why the representations in Fig. 6 are the patterns of the correlation coefficients instead of the original EOF patterns is because the former representation can visualize the relationship between the North Pacific and the North Atlantic but the latter expresses only the patterns in the North Pacific or the North Atlantic. The first modes in both the North Pacific and the North Atlantic are distributed widely, covering the eastern parts and lower latitudes of each ocean basin. The percent variances relative to the total are greater than 30%, respectively. The second mode in the North Pacific expresses a fluctuation at mainly southwestern regions, and the third mode is band-shaped depending on latitude. On the other hand, the second mode in the North Atlantic has a band shape depending on the latitude, and the third mode is distributed in the southwestern and northeastern regions of the North Atlantic.

As shown in the figures, the three dominant modes in both oceans show three characteristic distributions: 1) the eastern part of the basin, 2) the southwestern part of the basin, and 3) the band-shaped regions. The total percentage of variance in the three dominant modes is 55%–60%; these modes can be regarded as the major modes by EOF analysis.

The relation between the three dominant modes of the SWH and teleconnection patterns is discussed. Table 3 shows the correlation coefficients between the temporal coefficients of the three modes and the teleconnection pattern indices. For the North Pacific, the temporal coefficient of the first mode correlates significantly with the
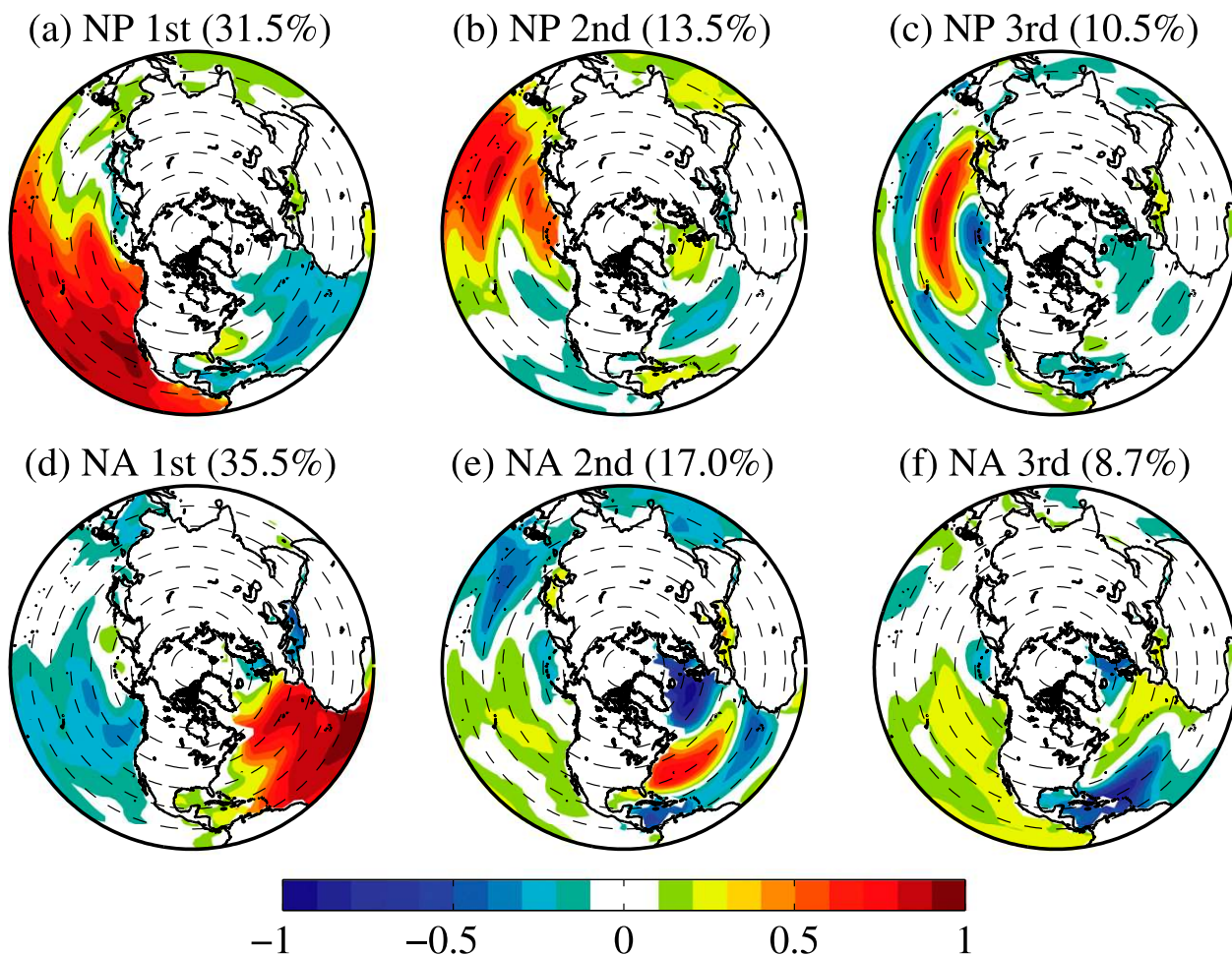
FIG. 6. Spatial distributions of EOFs of winter monthly average SWH in the North Pacific (NP) and the North Atlantic (NA). The percentage in parentheses indicates percent variance.

PNA, TNH, and Niño-3.4 indices. The first mode in the North Pacific indicates that SWH fluctuations are forced by fluctuations in the following: trade winds at lower latitudes, westerly winds at midlatitudes, and southward winds in the eastern North Pacific. Niño-3.4 impacts the trade winds. The PNA impacts the westerly winds, and the remaining TNH influences the southward winds in the eastern part of the North Pacific. The linearly combined index of three indices mentioned above is correlated well with the first mode, and the correlation coefficient is about 0.7.

On the other hand, the second mode has a significant correlation with the EPNP. The third mode is highly related to the WP, and the correlation coefficient is −0.8; this value is the highest among all the indices. This relationship between the third mode and the WP is discussed in detail in the next subsection.

The EOF results for the North Atlantic can be summarized as follows. The first mode, which includes fluctuation in the eastern part of the North Atlantic, is associated with the EA. The second mode shows band-shaped fluctuations that exhibit high correlation with the NAO; the correlation coefficient is −0.86.

The above discussion of the EOF and teleconnection pattern indices in the North Pacific and North Atlantic clearly indicates that the winter-averaged SWH values have similar spatial patterns of fluctuation in both ocean basins. Also, the spatial patterns of fluctuation, especially the band-shaped ones, correspond well to teleconnection patterns.

e. Winter wave climate variability in the North Pacific

The main spatial patterns (EOFs) of wave climate variability in the North Atlantic have been associated with the NAO (Wang and Swail 2001; Woolf et al. 2002; Gulev and Grigorieva 2006; Semedo et al. 2011) and EA (Woolf et al. 2002), and those in the North Pacific have been associated with the NPI (Gulev and Grigorieva

TABLE 3. Correlation coefficients between EOFs for winter monthly averaged SWH and teleconnection pattern indices. Values in bold typeface indicate that the correlation is statistically significant at the 5% significance level.

	NAO	EA	WP	EPNP	PNA	EAWR	SCA	TNH	POL	Niño-3.4	AO
North Pacific											
1st	0.01	−0.03	0.35	0.06	**0.46**	−0.17	−0.08	**−0.55**	−0.06	**0.44**	−0.00
2nd	0.31	−0.01	0.12	**−0.41**	−0.20	0.01	0.10	0.17	−0.18	−0.03	0.21
3rd	−0.08	−0.26	**−0.80**	0.37	**0.40**	−0.18	−0.09	0.03	−0.09	−0.11	**−0.37**
North Atlantic											
1st	−0.18	**0.62**	0.01	0.04	−0.29	0.34	0.29	**0.41**	−0.08	0.14	0.00
2nd	**−0.86**	−0.23	−0.08	0.24	0.17	−0.20	−0.03	−0.34	−0.16	0.19	**−0.75**
3rd	−0.23	0.35	−0.08	0.26	0.29	−0.19	0.26	−0.15	−0.01	0.18	−0.23

2006; Semedo et al. 2011), which is related to the PNA as described in the introduction, and the SOI (Semedo et al. 2011), which is related to El Niño. In addition, TNH, EPNP, and WP have been significantly associated with the main spatial patterns of wave climate variability in previous subsection. In particular, the band-shaped fluctuation of the SWH in the North Pacific, which is the third EOF mode, showed a strong connection to the WP. This relationship has not been discussed in previous studies. Therefore, the characteristics of the band-shaped fluctuation in the North Pacific are analyzed in detail and compared with observations. The third EOF mode of the SWH in the North Pacific is simply denoted NP3 in this section. The percent variance of NP3 is only 10.5% (Fig. 6) over the North Pacific, and thus one could consider NP3 to be negligible as wave climate variability. However, the contribution of NP3 becomes as high as 42% in limited regions such as 20°–40°N, 140°E–150°W.

For validation, we selected observed winter wave data by buoy and ship for analysis. The above discussion roughly covers an area of length scale 5000–10 000 km; therefore, data should be spread to a similar spatial scale for comparison. We selected six offshore buoys around the North Pacific as shown in Fig. 7. Two buoys [World Meteorological Organization (WMO) numbers 21001 and 21004] are maintained by the Japan Meteorological Agency (available at http://www.data.kishou.go.jp/kaiyou/db/vessel_obs/data-report/html/buoy/buoy_NoS2_e.html). The rest of the four buoys (WMO numbers 46003, 46006, 46035, and 51004) are maintained by the U.S. National Oceanographic Data Center (available at http://www.ndbc.noaa.gov/hmd.shtml). The periods of observation at buoys 21001, 21004, 46003, 46006, 46035, and 51004 are 1978–89, 1982–2000, 1976–98, 1977–2009, 1985–2009, and 1984–2008, respectively. In addition, ship observations by the International Comprehensive Ocean–Atmospheric Data Set (ICOADS; Woodruff et al. 2010) were added to the analysis. The ICOADS covers the region 27.5°–32.5°N, 162.5°–167.5°E over the period 1958–2009. The monthly averaged SWH observations used for the analysis and the locations of the three different sources are shown in Fig. 7.

The locations of buoys 21001 and 21004 are in the region where the NP3 shows positive values and the rest of the station locations are in the region with negative values (see Figs. 6c and 7). The location of the ICOADS is in the region where the NP3 shows strong positive values among all the locations (Figs. 6c and 7). The
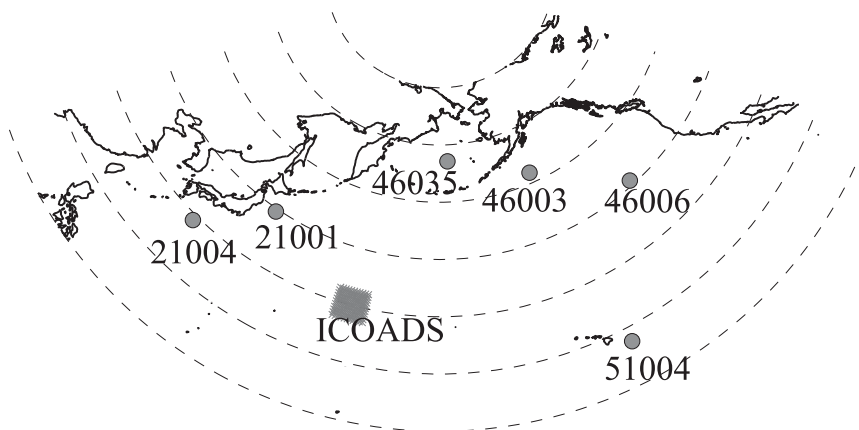

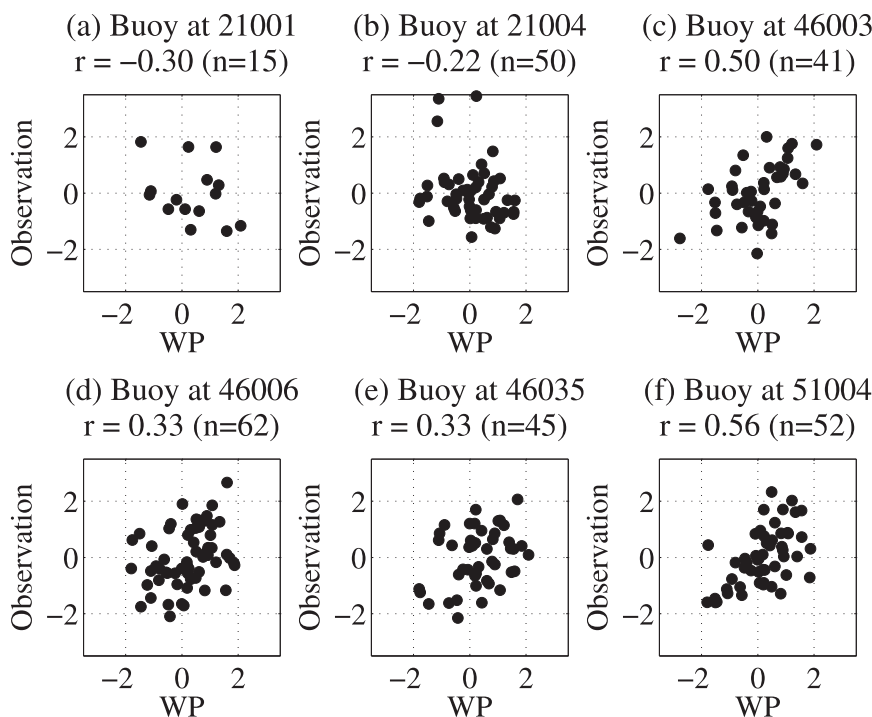FIG. 7. Locations of observation in the North Pacific.

FIG. 8. Relation between WP index and winter monthly average SWH derived from buoy observation data.

monthly averaged values cannot be calculated easily because of missing data in the observations. Therefore, only the monthly averages for those months when the ratio of missing data is less than 10% were used for analysis.

Additionally, the ICOADS observations are reported irregularly. Therefore, only the monthly averages for those months when the ratio of missing data is less than the average were used for analysis.

As a result, the total numbers of valid observations of monthly averaged SWH at buoys 21001, 21004, 46003, 46006, 46035, and 51004 and ICOADS are 15, 50, 41, 62, 45, 52, and 55, respectively. The monthly averages were standardized by each calendar month value. The observations of monthly averaged SWH values by buoy or ICOADS are plotted against the WP index in Figs. 8 and 9. Here, this WP index was derived from NCEP–NCAR reanalysis because observations cover a period longer than the ERA-40 period. The correlation coefficients at buoys 21001, 21004, 46003, 46006, 46035, and 51004 are −0.30, −0.22, 0.50, 0.33, 0.33, and 0.56, respectively.

The highest correlation coefficient of the ICOADS is −0.66. The locations where the correlation coefficients are positive are regions where the NP3 shows negative values, and vice versa. In addition, the magnitude of the correlation coefficient agrees with the magnitude of Fig. 6c at each location. This means that the NP3 is solidly related to the WP.

The relationship between the WP and the NP3 can also be discussed from a physical point of view. It is possible to explain the simultaneous fluctuations of the westerly and trade winds by Wallace et al. (1990) to some extent. Averaged winter SLP climatology in the North Pacific is characterized by higher values along the 20°–30°N line. Westerly winds are caused by pressure gradients between areas north of the line and the trade wind in the south. When the WP index is positive, the SLP becomes larger around the 20°–40°N region. Then the pressure gradient in this region becomes large, which causes the trade wind and westerly winds to be stronger at the same time. The opposite case is also possible. A strengthened (weakened) trade and westerly winds strengthen (weaken) waves zonally. As a result, the NP3 becomes the band-shaped distribution shown in Fig. 6c.

However, it is hard to explain the fluctuations of the SWH along 30°N by SLP climatology with the trade wind and westerly wind relationship. Therefore, we analyzed the relationship between extratropical cyclones and the NP3 along 30°N.

The extratropical cyclone data were culled from the winter SLP data in the ERA-40 reanalysis dataset from 1958 to 2001 based on the method of Geng and Sugi (2001). The definition of an extratropical cyclone is described as follows:
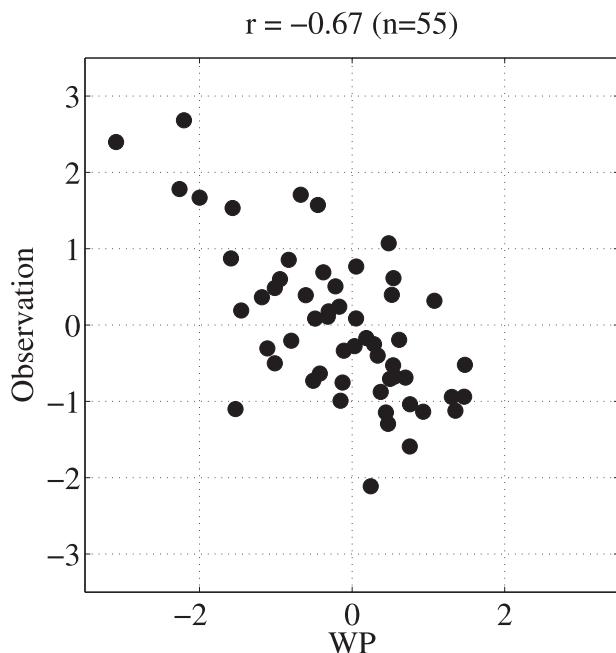
$$r = -0.67 \ (n=55)$$

FIG. 9. Relation between WP index and winter monthly average SWH derived from ICOADS observation data.

1) Atmospheric pressure is less than 1010 hPa.
2) Pressure is less than that of the surrounding eight grid points.
3) The averaged difference with the surrounding grid points is greater than 0.3 hPa.
4) Data on land are not used.
5) In cases where an extratropical cyclone satisfies the conditions listed above at a location 600 km or less from a grid point where an extratropical cyclone existed 1 time step (6 h) before, the two are defined as the same cyclone.

Figure 10 shows extratropical cyclone tracks (denoted storm tracks hereafter) in a representative month when the WP index is a positive or negative maximum. In cases where the WP index is positive, the storm track shifts northward. On the other hand, in cases where the WP index is negative, the storm track shifts southward and the area extends to a more easterly direction. The months when the WP index is more than 0.5 and less than −0.5 are divided into separate groups, and the monthly average number of storm tracks was counted. Figure 11 shows the difference between the positive and negative WP conditions (smoothed by 4° × 4°). Storm tracks shift either north or south depending on the WP index. When the WP index is positive, the storm does not have an effect on the region along 30°N, and vice versa. Therefore, fluctuation in the SWH along 30°N occurs depending on the extratropical cyclone activity, which depends on the sign of the WP.

Storm detection based on unfiltered SLP has bias because unfiltered SLP is strongly influenced by large spatial scales, such as the Icelandic low, and strong background flow (Hoskins and Hodges 2002). On the other hand, the vorticity field is less influenced by background flow. Therefore, storm detection based on relative vorticity at 850 hPa was also conducted. As a result, the relation between the WP and storm tracks is almost consistent with the results derived from storm detection based on unfiltered SLP, such as the storm track shifting either north or south depending on the WP index.

Lastly, another surface climate variability associated with the WP is discussed briefly. As an example, the increase in sea surface temperature south of Japan should be selected for discussion. As shown above, trade winds are strengthened when the WP index is positive. In addition, the southerly wind in the west reaches of the
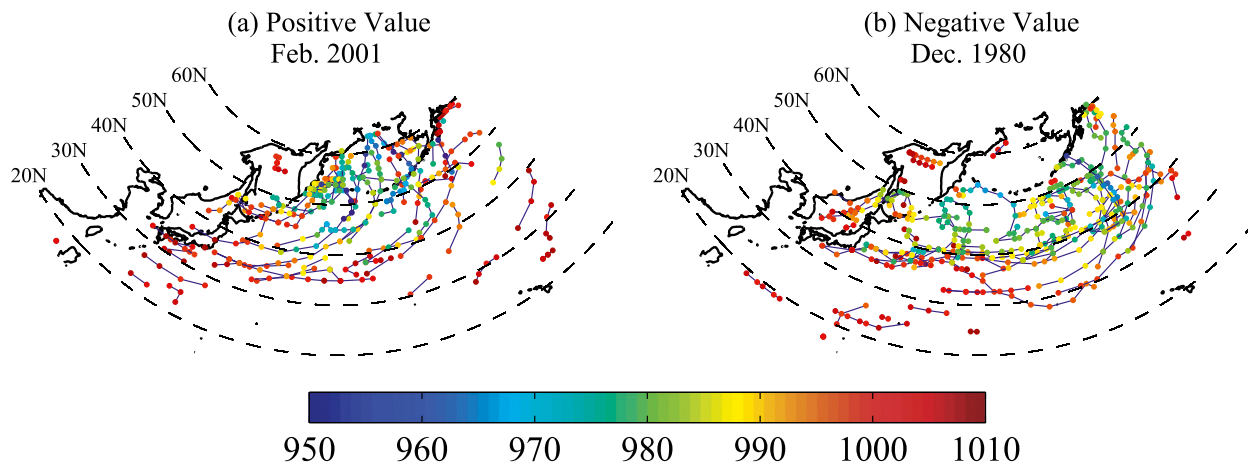

FIG. 10. Storm tracks in a representative month when the WP index showed (a) positive or (b) negative value (color coding indicates the atmospheric pressure in hPa).
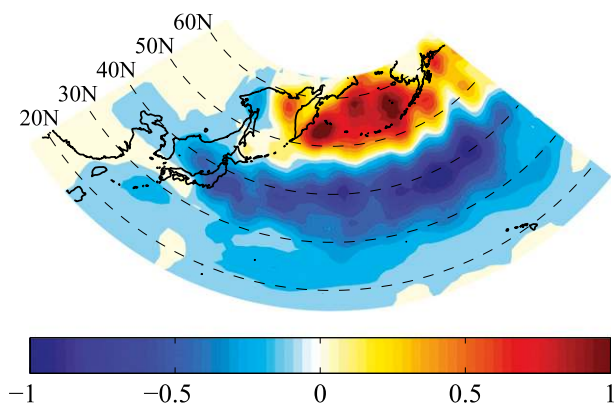
FIG. 11. The difference in the number of extratropical cyclones (winter storms) passing as classified by the WP index: (WP > 0.5) minus (WP < −0.5).

trade wind in the North Pacific is strengthened. As a result, heat is transported from south to north, and SST is increased in the South China Sea and along 30°N in the western North Pacific (Ose 2000; Wallace et al. 1990). Winter monthly averaged SST values in the regions 25°–30°N and 130°–160°E correlate well with WP indices in the ERA-40, and the correlation coefficient is 0.59. In this way, several climate variabilities can be associated with each other through teleconnection patterns.

4. Conclusions

The preferred pattern of large-scale climate variability is called a teleconnection pattern. Understanding the nature of teleconnection patterns and changes in their behaviors is central to understanding regional climate variability and climate change (Trenberth et al. 2007). This study provides comprehensive insight into the relationship between wave climate variability and teleconnection patterns, which has been studied before in a spatially limited way. The large-scale spatial patterns of wave heights on a monthly scale corresponding to teleconnection patterns in the Northern Hemisphere were discussed using reanalysis data.

Analysis was focused on the winter season because that season exhibits the strongest connection between wave height variability and teleconnection patterns as shown in section 3a. At first, the spatial distributions of wave height variability as influenced by several teleconnection patterns were identified by correlation analysis between monthly mean wave height and teleconnection pattern indices (Figs. 2 and 4). The wave response to teleconnection patterns makes sense in the eastern part of the ocean in the Northern Hemisphere because of a smooth relationship with atmospheric variations in this area. The relationship between wave climate variability

and teleconnection patterns strongly depends on the location (Fig. 3).

Second, the predictability of winter averaged SWH from a combination of teleconnection pattern indices was considered. As a result, the winter averaged SWH in some areas in the eastern part of the ocean can be estimated from a combination of teleconnection pattern indices. However, in areas such as those along 20° and 40°N in the western part of the North Pacific and 20°N in the western part of the North Atlantic, the winter averaged SWH cannot be evaluated well.

Third, the main spatial patterns of wave climate variability were analyzed by adapting EOF analysis to winter averaged SWH in the North Pacific and the North Atlantic respectively. The winter averaged SWH values have similar spatial patterns of fluctuation across both oceans. The spatial patterns of fluctuation, especially the band-shaped pattern, exhibit a strong relation to the teleconnection pattern. The characteristics of the band-shaped pattern of the SWH in the North Pacific were investigated in detail and found to be related to the WP pattern. The tracks of extratropical cyclones are related to the WP pattern in the region along 30°N. The fluctuation of the SWH along 30°N occurs depending on the extratropical cyclone activity, which depends on the phase of the WP pattern.

Semedo et al. (2011) investigated the leading modes of variability of wind-sea and swell based on the ERA-40 dataset, and swell plays an important role in the Northern Hemisphere. We did not separate wind-sea from swell in this study, and swell has different spatial distributions compared to wind seas. We will examine swell data in a similar fashion in the near future.

In this study wave climate has not been addressed in the context of climate change through teleconnection patterns, which is the next step of this study. However, this is discussed briefly, referring to some studies about future climate projection, focusing on the North Pacific in section 3e. Wang and Swail (2006) and Graham et al. (2013) show the winter wave height change under a forcing scenario at the end of the twenty-first century, indicating that future winter waves become small over the lower midlatitudes of the North Pacific, particularly in the central and western regions, and increase at higher latitudes. Mori et al. (2010) also show a similar change in the pattern of future wave heights over the North Pacific. Although Mori et al. (2010) analyzed annual average future changes, the pattern is dominated by winter changes. The future change pattern of winter wave heights over the North Pacific seen in Wang and Swail (2006), Graham et al. (2013), and Mori et al. (2010) is similar to the negative phase pattern for the NP3 (Fig. 6c), which is well associated with the WP pattern. Therefore, it can be

speculated that future forcing would increase the positive phase of the WP pattern, and then the change in the WP would lead to an increase in the negative phase of the NP3 because of the strong negative correlation between the NP3 and the WP pattern index. Furthermore, Fischer-Bruns et al. (2005) and Bengtsson et al. (2006) investigated the future change of storm tracks under a forcing scenario and showed that the change in frequency of winter storms over the North Pacific is characterized by a decrease at lower midlatitudes and an increase at higher latitudes, which is similar to Fig. 11 of this study. Therefore, the changes in storm tracks (Fischer-Bruns et al. 2005; Bengtsson et al. 2006) support the idea that future forcing would increase the positive phase of the WP pattern. This topic of future climate projection will be examined in detail in the near future.

REFERENCES

Akaike, H., 1973: Information theory and an extension of the maximum likelihood principle. *Proceedings of the Second International Symposium on Information Theory,* Vol. 1, B. N. Petrov and F. Caski, Eds., Akademiai Kiado, Budapest, 267–281.

Barnston, A., and R. Livezey, 1987: Classification, seasonality and persistence of low-frequency atmospheric circulation patterns. *Mon. Wea. Rev.,* **115,** 1083–1126.

Bauer, E., 2001: Interannual changes of the ocean wave variability in the North Atlantic and in the North Sea. *Climate Res.,* **18,** 63–69.

Bengtsson, L., K. Hodges, and E. Roeckner, 2006: Storm tracks and climate change. *J. Climate,* **19,** 3518–3543.

Bindoff, N., and Coauthors, 2007: Observations: Oceanic climate change and sea level. *Climate Change 2007: The Physical Science Basis,* S. Solomon et al., Eds., Cambridge University Press, 385–432.

Deser, C., A. Phillips, V. Bourdette, and H. Teng, 2012: Uncertainty in climate change projections: The role of internal variability. *Climate Dyn.,* **38,** 527–546.

Fan, Y., S.-J. Lin, I. M. Held, Z. Yu, and H. L. Tolman, 2012: Global ocean surface wave simulation using a coupled atmosphere–wave model. *J. Climate,* **25,** 6233–6252.

Fischer-Bruns, I., H. Storch, J. González-Rouco, and E. Zorita, 2005: Modelling the variability of midlatitude storm activity on decadal to century time scales. *Climate Dyn.,* **25,** 461–476.

Geng, Q., and M. Sugi, 2001: Variability of the North Atlantic cyclone activity in winter analyzed from NCEP–NCAR reanalysis data. *J. Climate,* **14,** 3863–3873.

Graham, N., and H. Diaz, 2001: Evidence for intensification of North Pacific winter cyclones since 1948. *Bull. Amer. Meteor. Soc.,* **82,** 1869–1893.

——, D. Cayan, P. Bromirski, and R. Flick, 2013: Multi-model projections of twenty-first century North Pacific winter wave climate under the IPCC A2 scenario. *Climate Dyn.,* **40,** 1335–1360, doi:10.1007/s00382-012-1435-8.

Gulev, S., and V. Grigorieva, 2006: Variability of the winter wind waves and swell in the North Atlantic and North Pacific as revealed by the voluntary observing ship data. *J. Climate,* **19,** 5667–5685.

Hawkins, E., and R. Sutton, 2009: The potential to narrow uncertainty in regional climate predictions. *Bull. Amer. Meteor. Soc.,* **90,** 1095–1107.

Hemer, M., J. Church, and J. Hunter, 2010: Variability and trends in the directional wave climate of the Southern Hemisphere. *Int. J. Climatol.,* **30,** 475–491.

Hoskins, B., and K. Hodges, 2002: New perspectives on the Northern Hemisphere winter storm tracks. *J. Atmos. Sci.,* **59,** 1041–1061.

Hurrell, J., 1996: Influence of variations in extratropical wintertime teleconnections on Northern Hemisphere temperature. *Geophys. Res. Lett.,* **23,** 665–668.

——, Y. Kushnir, G. Ottersen, and M. Visbeck, 2003: An overview of the North Atlantic oscillation. *The North Atlantic Oscillation: Climatic Significance and Environmental Impact, Geophys. Monogr.,* Vol. 134, Amer. Geophys. Union, 1–35.

Izaguirre, C., F. Mendez, M. Menendez, A. Luceño, and I. Losada, 2010: Extreme wave climate variability in southern Europe using satellite data. *J. Geophys. Res.,* **115,** C04009, doi:10.1029/2009JC005802.

——, ——, ——, and I. Losada, 2011: Global extreme wave height variability based on satellite data. *Geophys. Res. Lett.,* **38,** L10607, doi:10.1029/2011GL047302.

Kaiser, H., 1958: The varimax criterion for analytic rotation in factor analysis. *Psychometrika,* **23,** 187–200.

Kalnay, E., and Coauthors, 1996: The NCEP/NCAR 40-Year Reanalysis Project. *Bull. Amer. Meteor. Soc.,* **77,** 437–471.

Mase, H., R. Tanaka, N. Mori, and T. Yasuda, 2009: Long-term variability of annual large waves along coasts of the Sea of Japan (in Japanese). *J. Japan. Soc. Civ. Eng.,* **65,** 1251–1255, doi:10.2208/kaigan.65.1251.

McPhaden, M., S. Zebiak, and M. Glantz, 2006: ENSO as an integrating concept in earth science. *Science,* **314,** 1740–1745.

Menéndez, M., F. Méndez, I. Losada, and N. Graham, 2008: Variability of extreme wave heights in the northeast Pacific Ocean based on buoy measurements. *Geophys. Res. Lett.,* **35,** L22607, doi:10.1029/2008GL035394.

Mori, N., T. Yasuda, H. Mase, T. Tom, and Y. Oku, 2010: Projection of extreme wave climate change under global warming. *Hydrol. Res. Lett.,* **4,** 15–19, doi:10.3178/hrl.4.15.

Ose, T., 2000: A biennially oscillating sea surface temperature and the western Pacific pattern. *J. Meteor. Soc. Japan,* **78,** 93–99.

Panagiotopoulos, F., M. Shahgedanova, and D. Stephenson, 2002: A review of Northern Hemisphere winter-time teleconnection patterns. *J. Phys. IV,* **12,** 1027–1047.

Semedo, A., K. Sušelj, A. Rutgersson, and A. Sterl, 2011: A global view on the wind sea and swell climate and variability from ERA-40. *J. Climate,* **24,** 1461–1479.

Seymour, R., 2011: Evidence for changes to the northeast Pacific wave climate. *J. Coast. Res.,* **27,** 194–201.

Sterl, A., and S. Caires, 2005: Climatology, variability and extrema of ocean waves: The Web-based KNMI/ERA-40 wave atlas. *Int. J. Climatol.,* **25,** 963–977.

Tebaldi, C., J. Arblaster, and R. Knutti, 2011: Mapping model agreement on future climate projections. *Geophys. Res. Lett.,* **38,** L23701, doi:10.1029/2011GL049863.

Thompson, D., and J. Wallace, 1998: The Arctic Oscillation signature in the wintertime geopotential height and temperature fields. *Geophys. Res. Lett.,* **25,** 1297–1300.

Tokinaga, H., and S. Xie, 2011: Wave- and anemometer-based sea surface wind (WASWind) for climate change analysis. *J. Climate,* **24,** 267–285.

Trenberth, K., 1990: Recent observed interdecadal climate changes in the Northern Hemisphere. *Bull. Amer. Meteor. Soc.,* **71,** 988–993.

——, and J. Hurrell, 1994: Decadal atmosphere–ocean variations in the Pacific. *Climate Dyn.,* **9,** 303–319.

——, J. Caron, D. Stepaniak, and S. Worley, 2002: Evolution of El Niño–Southern Oscillation and global atmospheric surface temperatures. *J. Geophys. Res.,* **107,** 4065, doi:10.1029/2000JD000298.

——, and Coauthors, 2007: Observations: Surface and atmospheric climate change. *Climate Change 2007: The Physical Science Basis,* S. Solomon et al., Eds., Cambridge University Press, 235–336.

Uppala, S., and Coauthors, 2005: The ERA-40 Re-Analysis. *Quart. J. Roy. Meteor. Soc.,* **131,** 2961–3012.

von Storch, H., and F. Zwiers, 2002: *Statistical Analysis in Climate Research.* Cambridge University Press, 484 pp.

Walker, G., and E. Bliss, 1932: World weather V. *Mem. Roy. Meteor. Soc.,* **4,** 53–84.

Wallace, J., and D. Gutzler, 1981: Teleconnections in the geopotential height field during the Northern Hemisphere winter. *Mon. Wea. Rev.,* **109,** 784–812.

——, C. Smith, and Q. Jiang, 1990: Spatial patterns of atmosphere–ocean interaction in the northern winter. *J. Climate,* **3,** 990–998.

Wang, X., and V. Swail, 2001: Changes of extreme wave heights in Northern Hemisphere oceans and related atmospheric circulation regimes. *J. Climate,* **14,** 2204–2221.

——, and ——, 2006: Climate change signal and uncertainty in projections of ocean wave heights. *Climate Dyn.,* **26,** 109–126.

Woodruff, S., and Coauthors, 2010: ICOADS release 2.5: Extensions and enhancements to the surface marine meteorological archive. *Int. J. Climatol.,* **31,** 951–967.

Woolf, D., P. Challenor, and P. Cotton, 2002: Variability and predictability of the North Atlantic wave climate. *J. Geophys. Res.,* **107,** 3145, doi:10.1029/2001JC001124.